J|A|C|S
ARTICLES

Published on Web 11/20/2008

Intramolecular Valence and Spin Interaction in *meso* and *rac* Diastereomers of a *p*-Quinonoid-Bridged Diruthenium Complex

Doyel Kumbhakar,[†] Biprajit Sarkar,[‡] Somnath Maji,[†] Shaikh M. Mobin,[†] Jan Fiedler,[§] Francisco A. Urbanos,[⊥] Reyes Jiménez-Aparicio,*[,⊥] Wolfgang Kaim,*[,‡] and Goutam Kumar Lahiri*[,†]

Department of Chemistry, Indian Institute of Technology Bombay, Powai, Mumbai-400076, India, Institut für Anorganische Chemie, Universität Stuttgart, Pfaffenwaldring 55, D-70550 Stuttgart, Germany, J. Heyrovský Institute of Physical Chemistry, v.v.i., Academy of Sciences of the Czech Republic, Dolejškova 3, CZ-18223 Prague, Czech Republic, and Departamento de Química Inorgánica, Facultad de Ciencias Químicas, Universidad Complutense, Ciudad Universitaria, E-28040 Madrid, Spain

Received September 11, 2008; E-mail: kaim@iac.uni-stuttgart.de; lahiri@chem.iitb.ac.in

Abstract: The complexes *meso*- and *rac*-$[(acac)_2Ru(\mu\text{-}L)Ru(acac)_2]^n$, **1** and **2**, where L^{2-} = 1,4-dioxido-2,3-bis(3,5-dimethylpyrazol-1′-yl)benzene and $acac^-$ = 2,4-pentanedionato, were characterized structurally, magnetically, electrochemically, and spectroscopically as well as spectroelectrochemically (UV−vis−NIR, EPR) in the accessible redox states (n = 0, +, −, 2−). Due to steric interference, the neutral compounds contain a severely twisted L^{2-} bridging ligand with 43−48° dihedral angles between the planes of the hydroquinone dianion and those of the *ortho* positioned pyrazolyl substituents. The difference between *meso* and *rac* isomers is rather pronounced in terms of the redox potentials (easier oxidation *and* reduction of the *rac* form **2**) and with respect to the absorption spectra of the oxidized states. Susceptibility and EPR measurements confirm the $\{Ru^{III}(\mu\text{-}L^{2-})Ru^{III}\}$ configuration of the neutral species, showing J values of −37 and −21 cm^{-1} for the spin−spin interaction between the ca. 7.75 Å separated metal centers in **1** and **2**, respectively. Two-step reduction involves the metals and produces $Ru^{III}Ru^{II}$ mixed-valent monoanions with comproportionation constants of ca. 10^4, with Ru^{III}-type EPR signals, and with broad intervalence charge transfer bands at about 1200−1500 nm absorption maximum, suggesting localized valence (class II). Oxidation produces intense near-infrared absorption at 892 ($\mathbf{1}^+$) or 1027 nm ($\mathbf{2}^+$) and narrow isotropic EPR spectra at $g \approx 2.005$, signifying unprecedented spin localization at the *p*-semiquinone bridge. These results are not compatible with an (L^{2-})-bridged $\{Ru^{IV}Ru^{III}\}$ situation nor with an $\{Ru^{III}(\mu\text{-}L^{\bullet-})Ru^{III}\}$ three-spin arrangement with up−down−up spin configuration in the ground state, which would result in metal-centered spin through antiferromagnetic coupling between the adjacent individual spins. Only the $\{Ru^{III}(\mu\text{-}L^{\bullet-})Ru^{III}\}$ situation, with up−up−down spin configuration, leads to ligand-centered resulting spin through the strong antiferromagnetic coupling between the remote metal spins, an unusual situation which is favored here because of weakened metal−radical coupling resulting from the pyrazolyl/*p*-semiquinone twist.

Introduction

As naturally occurring redox-active molecules, the quinones are widely distributed, functioning in vital electron transport processes where they often interact with transition metal ions[1a,b] or exhibit specific toxicity.[1c] *ortho*-Quinone-containing prosthetic groups in metallo-quinoproteins (Chart 1) are well known in the form of pyrrolo-quinoline-quinone (PQQ), tryptophan-tryptophyl-quinone (TTQ), topaquinone (TPQ), and lysine-tyrosyl-quinone (LTQ).[2] Catechols as $2e^-/2H^+$-reduced *o*-quinones are being investigated as antioxidants (polyphenols), as neurotransmitters (catecholamines), and as precursors of melanin pigments.[3]

However, *para*-quinones (Chart 2) such as vitamin K derivatives, ubiquinones, or plastoquinones also play many important roles in energy conversion (photosynthesis, respiration) and information transfer.[3,4]

In order to rationalize the intricate electronic interactions between transition metal ions and quinone redox systems in biochemical environments, there have been considerable inves-

[†] Indian Institute of Technology Bombay.
[‡] Universität Stuttgart.
[§] Academy of Sciences of the Czech Republic.
[⊥] Universidad Complutense.

(1) (a) Nohl, H.; Jordan, W.; Youngman, R. I. *Adv. Free Rad. Biol. Med.* **1986**, *2*, 211. (b) Thomson, S. D. *Naturally Occurring Quinones IV*; Springer: The Netherlands, 1996. (c) Bolton, J. L.; Trush, M. A.; Penning, T. M.; Dryhurst, G.; Monks, T. J. *Chem. Res. Toxicol.* **2000**, *13*, 135.

(2) (a) Duine, J. A.; Jongejan, J. A. In *Bioinorganic Catalysis*; Reedijk, J., Ed.; Marcel Dekker: New York, 1993; p 447. (b) Klinman, J. P. *Proc. Natl. Acad. Sci. U.S.A.* **2001**, *98*, 705. (c) Mure, M.; Mills, S. A.; Klinman, J. P. *Biochemistry* **2002**, *41*, 9269. (d) Wang, S. X.; Nakamura, N.; Murell, M.; Klinman, J. P.; Sanders-Loehr, J. *J. Biol. Chem.* **1997**, *272*, 28841. (e) Mure, M.; Wang, S. X.; Klinman, J. P. *J. Am. Chem. Soc.* **2003**, *125*, 6113. (f) Anthony, C. *Arch. Biochem. Biophys.* **2004**, *428*, 2. (g) Anthony, C. *Biochem. J.* **1996**, *320*, 697.

Chart 1

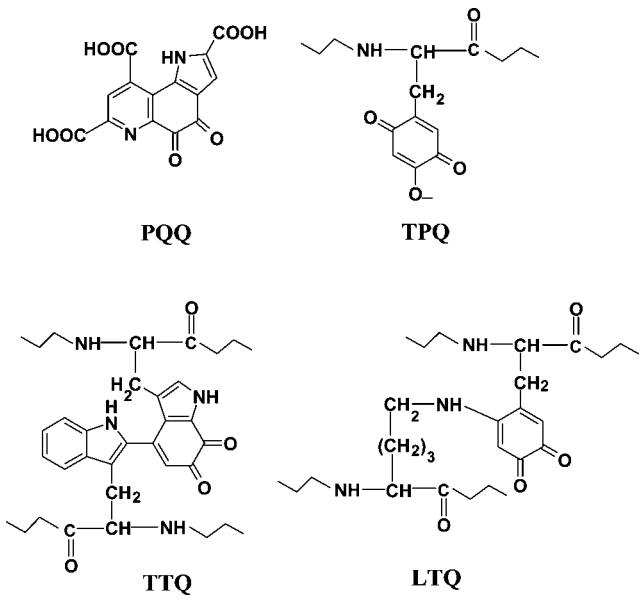

Chart 2

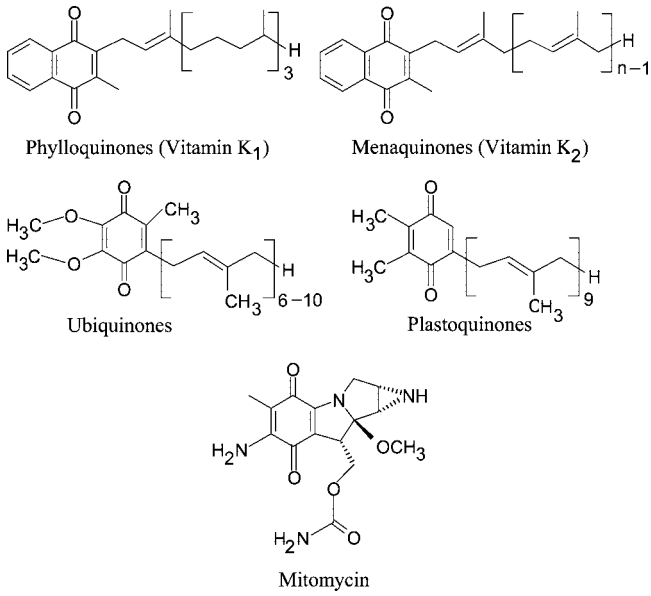

tigations at the molecular level of metal complexes with O,O′-chelating *o*-quinonoid ligands, particularly in assigning the valence state distribution at the metal−quinone interface.[5] However, despite the biochemical significance,[1,4] far fewer results have been reported for the coordination chemistry of *p*-quinonoid ligands,[6,7] including those with combined *o*,*p*-quinone functions.[6r−w] The present study is aimed at exploring the electronic structural aspects of two diastereomeric diruthenium compounds, [(acac)$_2$Ru(μ-L)Ru(acac)$_2$], **1** and **2** (Scheme 1), where L^{2-} is the two-electron-reduced *p*-quinonoid ligand 1,4-dioxido-2,3-bis(3,5-dimethylpyrazol-1′-yl)benzene and acac$^-$ = acetylacetonate = 2,4-pentanedionate. Although 1,4-dioxido-2,5-bis(pyrazol-1′-yl)benzene, $(L')^{2-}$, has been used previously

Scheme 1

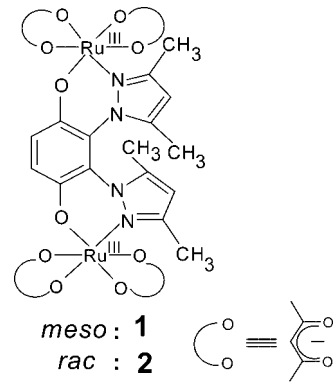

for the formation of polynuclear complexes,[6a−d] including [(bpy)$_2$Ru(μ-L′)Ru(bpy)$_2$]^n,[7e] the new compounds **1** and **2** represent the first set of polynuclear metal complexes bridged by L^{2-}.

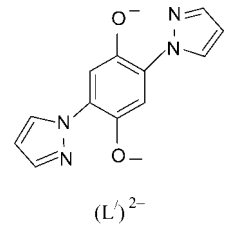

The preferential stabilization of ruthenium ions in the paramagnetic 3+ oxidation state in **1** or **2** via the σ-donation effect of anionic acac$^-$ and L^{2-} introduces the possibility of studying L^{2-}-mediated magnetic exchange between Ru^{III} centers. In addition, the initially ambivalent electronic situations in the one-electron-reduced form {Ru(μ-L)Ru}$^-$, as well as in the one-electron-oxidized state {Ru(μ-L)Ru}$^+$, were targets of our investigation. The present work thus describes the metal−ligand−metal valence state distributions in both the isolated neutral systems and the spectroelectrochemically accessible charged redox states of diastereomeric $\mathbf{1}^n$ and $\mathbf{2}^n$ (n = 0, +, −, 2−), using X-ray structure analysis, SQUID susceptometry, OTTLE spectroelectrochemistry, and EPR.

Results and Discussion

Synthesis and Characterization. The diastereomeric complexes [*meso* ($\Delta\Lambda$), **1**; *rac* ($\Delta\Delta/\Lambda\Lambda$), **2**][8] were isolated from the reaction of $Ru^{II}(acac)_2(CH_3CN)_2$ with 1,4-dihydroxy-2,3-bis(3,5-dimethylpyrazol-1′-yl)benzene (H_2L) in the presence of

(3) Izumi, Y.; Sawada, H.; Sakka, N.; Yamamoto, N.; Kume, T.; Katsuki, H.; Shimohama, S.; Akaike, A. *J. Neurosci. Res.* **2005**, *79*, 849.

(4) (a) Furie, B.; Bouchard, B. A.; Furie, B. C. *Blood* **1999**, *93*, 1798. (b) Meganathan, R. *Vitam. Horm.* **2001**, *61*, 173. (c) He, M.; Sheldon, P. J.; Sherman, D. H. *Proc. Natl. Acad. Sci. U.S.A.* **2001**, *98*, 926.

(5) (a) Pierpont, C. G.; Lange, C. W. *Prog. Inorg. Chem.* **1994**, *41*, 331. (b) Pierpont, C. G. *Coord. Chem. Rev.* **2001**, *219*−*221*, 415. (c) Lever, A. B. P.; Gorelsky, S. I. *Coord. Chem. Rev.* **2000**, *208*, 153. (d) Gorelsky, S. I.; Lever, A. B. P.; Ebadi, M. *Coord. Chem. Rev.* **2002**, *230*, 97. (e) Dei, A.; Gatteschi, D.; Sangregorio, C.; Sorace, L. *Acc. Chem. Res.* **2004**, *37*, 827. (f) Pierpont, C. G.; Attia, A. S. *Collect. Czech. Chem. Commun.* **2001**, *66*, 33. (g) DelMedico, A.; Dodsworth, E. S.; Lever, A. B. P.; Pietro, W. J. *Inorg. Chem.* **2004**, *43*, 2654. (h) da Cunha, C. J.; Dodsworth, E. S.; Monteiro, M. A.; Lever, A. B. P. *Inorg. Chem.* **1999**, *38*, 5399. (i) Salmonsen, R. B.; Abelleira, A.; Clarke, M. J. *Inorg. Chem.* **1984**, *23*, 385. (j) Patra, S.; Sarkar, B.; Mobin, S. M.; Kaim, W.; Lahiri, G. K. *Inorg. Chem.* **2003**, *43*, 6469. (k) Remenyi, C.; Kaupp, M. *J. Am. Chem. Soc.* **2005**, *127*, 11399. (l) Maji, S.; Patra, S.; Chakraborty, S.; Mobin, S. M.; Janardanan, D.; Sunoj, R. B.; Lahiri, G. K. *Eur. J. Inorg. Chem.* **2007**, 314. (m) Dei, A.; Gatteschi, D.; Pardi, L. *Inorg. Chim. Acta* **1991**, *189*, 125. (n) Frantz, S.; Rall, J.; Hartenbach, I.; Schleid, T.; Zalis, S.; Kaim, W. *Chem. Eur. J.* **2004**, *19*, 149.

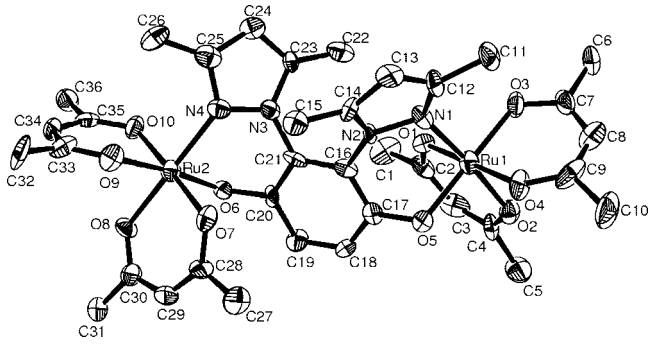

Figure 1. ORTEP diagram of **1**. Ellipsoids are drawn at 50% probability.

Table 1. Selected Crystallographic Data for **1** and **2**

	$1 \cdot 2H_2O$	$2 \cdot 2CH_2Cl_2$
mol formula	$C_{36}H_{48}N_4O_{12}Ru_2$	$C_{38}H_{48}Cl_4N_4O_{10}Ru_2$
fw	930.94	1064.74
cryst sym	tetragonal	monoclinic
space group	*P4/ncc*	$P2_1/n$
a (Å)	25.4585(4)	13.3882(3)
b (Å)	25.485(2)	11.5698(3)
c (Å)	24.7823(18)	28.3154(6)
β (deg)	90.00	92.939(2)
V (Å^3)	16078.9(19)	4380.25(18)
Z	16	4
μ (mm^{-1})	0.815	0.992
T (K)	120(2)	150(2)
D_{calcd} (g cm^{-3})	1.532	1.615
F (000)	7552	2160
2θ range (deg)	2.91−25.00	3.05−25.00
data/restraints/parameters	7092/0/502	7684/0/535
*R*1, w*R*2 [I > 2σ(*I*)]	0.0589, 0.0924	0.0344, 0.0727
*R*1, w*R*2 (all data)	0.1871, 0.1256	0.0494, 0.0794
GOF	0.805	1.050
largest diff. peak/hole (e Å^{-3})	1.030 and −0.571	0.543 and −0.529

NEt_3 as a base under aerobic conditions, followed by chromatographic separation using a neutral alumina column. The ligand L^{2-} bridges two complex fragments $\{Ru(acac)_2\}^+$, each through one anionic O^- and one neutral pyrazolyl N donor, forming two six-membered chelate rings.

The combined electron donor effects from chelating terminal $acac^-$ ligands and from the doubly deprotonated anionic hydroquinone moiety (L^{2-}) facilitate the isolation of ruthenium in the paramagnetic 3+ oxidation state in **1** and **2** under aerobic reaction conditions, as observed similarly for many other $\{Ru(acac)_2\}$ derivatives.[9,10]

The neutral diastereomers **1** and **2** are identified by their microanalytical data and by mass spectrometry (see Experimental Section). The paramagnetic **1** and **2** exhibit magnetic moments of about 2.4 μ_B at 298 K, which implies antiferromagnetic coupling of Ru^{III} (cf. below). Compounds **1** and **2** display complex EPR spectra in acetonitrile at 110 K as well as ^{1}H NMR resonances (at 298 K) over a wide range, between +30 and −40 ppm in $CDCl_3$ (Figures S1 and S2, Supporting Information), resulting from paramagnetic contact shift.[11] The *rac* isomer **2** shows signals due to four CH(acac), eight CH_3(acac), two CH(quinone), four CH_3(pyrazolyl), and two CH(pyrazolyl) protons corresponding to the full molecule, whereas the *meso* isomer **1** displays signals equivalent to half of the molecule.

Crystal Structures. The isomeric identity of **1** and **2** corresponding to *meso* and *rac*, respectively, has been evidenced by their crystal structures (Figures 1 and 2). Selected crystallographic parameters and comparative bond lengths and bond angles are given in Tables 1 and 2, respectively. Each ruthenium(III) ion is bonded to the bridging ligand (L^{2-}) through a pair of N,O$^-$ donors to form a six-membered chelate ring. The $Ru(1)O_5N$ and $Ru(2)O_5N$ arrangements in **1** and **2** are distorted octahedral. The Ru−O distances with the bridging L^{2-} in **1** [1.974(6)/1.965(6) Å] and in **2** [1.976(2)/1.983(2) Å] lie within a close range and are slightly shorter than the Ru−O bonds involving the $acac^-$ groups (average 2.000 and 2.018 Å in **1** and **2**, respectively). This observation suggests a less balanced charge from the chelate donor atoms in L^{2-}, as evident from the Ru−N distances: the longest bonds for each ruthenium(III) ion are those to the pyrazolyl nitrogen atoms of the bridging L^{2-} ligand at 2.069(7)/2.070(8) Å for **1** and at 2.059(3)/2.072(3) Å for **2**. In general, the bond lengths involving the metal ions of **1** and **2** are in the expected range.[12] The intramolecular

(6) (a) Kretz, T.; Bats, J. W.; Losi, S.; Wolf, B.; Lerner, H. -W.; Lang, M.; Zanello, P.; Wagner, M *Dalton Trans.* **2006**, 4914. (b) Margraf, G.; Kretz, T.; de Biani, F. F.; Laschi, F.; Losi, S.; Zanello, P.; Bats, J. W.; Wolf, B.; Removic-Langer, K.; Lang, M.; Prokofiev, A.; Assmus, W.; Lerner, H.-W.; Wagner, M. *Inorg. Chem.* **2006**, *45*, 1277. (c) Wolf, B.; Bruehl, A.; Pashchenko, V.; Removic-Langer, K.; Kretz, T.; Bats, J. W.; Lerner, H.-W.; Wagner, M.; Salguero, A.; Saha-Dasgupta, T.; Rahaman, B.; Valenti, R.; Lang, M. *C. R. Chim.* **2007**, *10*, 109. (d) Dinnebier, R.; Lerner, H.-W.; Ding, L.; Shankland, K.; David, W. I. F.; Stephens, P. W.; Wagner, M. *Z. Anorg. Allg. Chem.* **2002**, *628*, 310. (e) Siri, O.; Braunstein, P. *Chem. Commun.* **2000**, 2223. (f) Elduque, A.; Garces, Y.; Oro, L. A.; Pinillos, M. T.; Tiripicchio, A.; Ugozzoli, F. *J. Chem. Soc., Dalton Trans.* **1996**, 2155. (g) Dei, A.; Gatteschi, D.; Pardi, L.; Russo, U. *Inorg. Chem.* **1991**, *30*, 2589. (h) Calvo, M. A.; Lanfredi, A. M. M.; Oro, L. A.; Pinillos, M. T.; Tejel, C.; Tiripicchio, A.; Ugozzoli, F. *Inorg. Chem.* **1993**, *32*, 1147. (i) Johnston, R. F.; Holwerda, R. A. *Inorg. Chem.* **1985**, *24*, 153. (j) Vlcek, A. A.; Danzlik, J. *Inorg. Chem.* **1967**, *6*, 2053. (k) Liu, S.; Shaikh, S. N.; Zubieta, J. *Inorg. Chem.* **1989**, *28*, 723. (l) Folgado, J. V.; Ibanez, R.; Coronado, E.; Beltran, D.; Savariault, J. M.; Galy, J. *Inorg. Chem.* **1988**, *27*, 19. (m) Lloret, F.; Julve, M.; Faus, J.; Solans, X.; Journaux, Y.; Morgenstern-Badarau, I. *Inorg. Chem.* **1990**, *29*, 2232. (n) Pierpont, C. G.; Francescons, L. C.; Hendrickson, D. N. *Inorg. Chem.* **1978**, *17*, 3470. (o) Wrobleski, J. T.; Brown, D. B. *Inorg. Chem.* **1979**, *18*, 498. (p) Mathur, P.; Dismukes, G. C. *J. Am. Chem. Soc.* **1983**, *105*, 7093. (q) Cornago, P.; Escolastico, C.; Santa Maria, M. D.; Claramunt, R. M.; Carmona, D.; Esteban, M.; Oro, L. A.; Foces-Foces, C.; Llamas-Saiz, L.; Elguero, J. *J. Organomet. Chem.* **1994**, *467*, 293. (r) Min, K. S.; Rheingold, A. L.; DiPasquale, A.; Miller, J. S. *Inorg. Chem.* **2006**, *45*, 6135. (s) Min, K. S.; DiPasquale, A.; Rheingold, A. L.; Miller, J. S. *Inorg. Chem.* **2007**, *46*, 1048. (t) Guo, D.; McCusker, J. K. *Inorg. Chem.* **2007**, *46*, 3257. (u) Tao, J.; Maruyama, H.; Sato, O. *J. Am. Chem. Soc.* **2006**, *128*, 1790. (v) Min, K. S.; DiPasquale, A. G.; Golen, J. A.; Rheingold, A. L.; Miller, J. S. *J. Am. Chem. Soc.* **2007**, *129*, 2360. (w) Cotton, F. A.; Jin, J.-Y.; Li, Z.; Murillo, C. A.; Reibenspies, J. H. *Chem. Commun.* **2008**, 211.

(7) Ruthenium complexes: (a) Ernst, S.; Haenel, P.; Jordanov, J.; Kaim, W. V.; Kasack, V.; Roth, E. *J. Am. Chem. Soc.* **1989**, *111*, 1733. (b) Ghumaan, S.; Mukherjee, S.; Kar, S.; Roy, D.; Mobin, S. M.; Sunoj, R. B.; Lahiri, G. K. *Eur. J. Inorg. Chem.* **2006**, *21*, 4426. (c) Maji, S.; Sarkar, B.; Mobin, S. M; Fiedler, J.; Urbanos, F. A.; Jimenez-Aparicio, R.; Kaim, W.; Lahiri, G. K. *Inorg. Chem.* **2008**, *47*, 5204. (d) Kar, S.; Sarkar, B.; Ghumaan, S.; Janardanan, D.; van Slageren, J.; Fiedler, J.; Puranik, V. G.; Sunoj, R. B.; Kaim, W.; Lahiri, G. K. *Chem. Eur. J.* **2005**, *11*, 4901. (e) Keyes, T. E.; Forster, R. J.; Jayaweera, P. M.; Coates, C. G.; McGarvey, J. J.; Vos, J. G. *Inorg. Chem.* **1998**, *37*, 5925. (f) Bond, A. M.; Marken, F.; Williams, C. T.; Beattie, D. A.; Keyes, T. E.; Forster, R. J.; Vos, J. G. *J. Phys. Chem. B* **2000**, *104*, 1977. (g) Ward, M. D. *Inorg. Chem.* **1996**, *35*, 1712. (h) Dei, A.; Gatteschi, D.; Pardi, L. *Inorg. Chem.* **1990**, *29*, 1442. (i) Ura, Y.; Sato, Y.; Shiotsuki, M.; Suzuki, T.; Wada, K.; Kondo, T.; Mitsudo, T. -A *Organometallics* **2003**, *22*, 77.

(8) (a) Keene, F. R. *Chem. Soc. Rev.* **1998**, *27*, 185. (b) D'Alessandro, D. M.; Keene, F. R. *Chem. Phys.* **2006**, *324*, 8.

(9) Kar, S.; Sarkar, B.; Ghumaan, S.; Roy, D.; Urbanos, F. A.; Fiedler, J.; Sunoj, R. B.; Jimenez-Aparicio, R.; Kaim, W.; Lahiri, G. K. *Inorg. Chem.* **2005**, *44*, 8715.

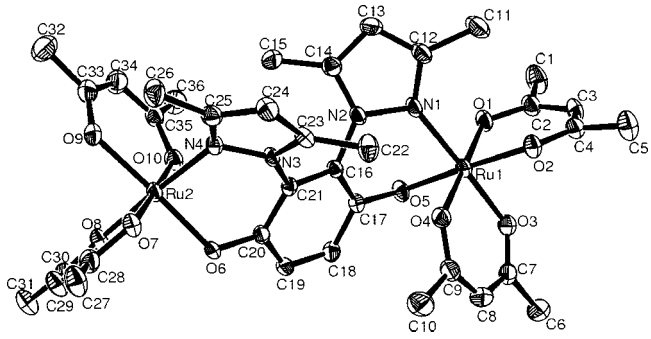

Figure 2. ORTEP diagram of **2**. Ellipsoids are drawn at 50% probability.

distances between the two paramagnetic metal centers in **1** and **2** are 7.709 and 7.771 Å, respectively.

The coordinated pyrazolyl rings are not coplanar with the *p*-quinone part of L^{2-}. The angles between the planes comprising the benzo ring and the pyrazolyl ring N3,N4,C23,C24,C25 are around 47.8° for both molecules, whereas the angles between the former and the second pyrazolyl ring (N1,N2,C12,C13,C14) are 45.8° and 42.9° in **1** and **2**, respectively. These values indicate a rather diminished π conjugation. The two pyrazolyl rings of L^{2-} are situated at angles of 46.3° and 54.7° in **1** and **2**, respectively.

Magnetic Properties. For both compounds, the change in magnetization with increase in the magnetic field at 5 or 300 K is linear, at least until 50 000 G. For both complexes, the magnetization values are lower than those predicted by the Brillouin function[13] for two paramagnetic centers, $S = {}^1/_2$ (g = 2.00) + $^1/_2$ (g = 2.00), suggesting the presence of antiferromagnetic interactions, mainly at low temperatures (Figures S3 and S4, Supporting Information).

The magnetic susceptibility curve of **1** versus temperature shows a broad maximum at 69 K (Figure 3a), supporting the presence of antiferromagnetic interactions. In addition, the susceptibility curve shows a typical paramagnetic tail at very low temperatures, ascribed to a small quantity of paramagnetic ($S = 1$) impurity, which is tentatively attributed to a noncoupled phase of the same compound. The magnetic moment of 2.40 μ_B at room temperature is close to that expected for the presence of two isolated unpaired electrons associated with two Ru^{III} ions per molecule. The μ_{eff} decreases from 2.40 to 0.33 μ_B at 2 K, in accordance with an antiferromagnetic interaction.

Table 2. Selected Bond Distances (Å) and Angles (°) in **1** and **2**

	1	2
	Bond Distances	
Ru(1)−O(1)	1.997(7)	2.032(2)
Ru(1)−O(2)	1.999(6)	2.016(2)
Ru(1)−O(3)	1.999(7)	2.020(2)
Ru(1)−O(4)	2.006(7)	2.004(2)
Ru(1)−O(5)	1.974(6)	1.976(2)
Ru(1)−N(1)	2.069(7)	2.072(3)
Ru(2)−O(6)	1.965(6)	1.983(2)
Ru(2)−O(7)	2.007(6)	2.017(2)
Ru(2)−O(8)	2.015(6)	2.042(2)
Ru(2)−O(9)	2.024(6)	2.018(2)
Ru(2)−O(10)	2.023(6)	2.024(2)
Ru(2)−N(4)	2.070(8)	2.059(3)
C(17)−O(5)	1.343(11)	1.347(4)
C(20)−O(6)	1.378(10)	1.346(4)
	Bond Angles	
O(5)−Ru(1)−O(1)	89.8(3)	89.98(9)
O(5)−Ru(1)−O(2)	86.9(3)	177.58(10)
O(1)−Ru(1)−O(2)	94.8(3)	90.62(9)
O(5)−Ru(1)−O(3)	177.4(3)	90.12(9)
O(1)−Ru(1)−O(3)	88.4(3)	86.72(9)
O(2)−Ru(1)−O(3)	91.3(3)	87.57(9)
O(5)−Ru(1)−O(4)	90.1(3)	89.62(9)
O(1)−Ru(1)−O(4)	178.0(2)	179.50(9)
O(2)−Ru(1)−O(4)	83.1(3)	89.80(9)
O(3)−Ru(1)−O(4)	91.6(3)	93.58(9)
O(5)−Ru(1)−N(1)	86.7(3)	85.94(10)
O(1)−Ru(1)−N(1)	88.9(3)	90.96(10)
O(2)−Ru(1)−N(1)	172.6(3)	96.39(10)
O(3)−Ru(1)−N(1)	95.2(3)	175.43(10)
O(4)−Ru(1)−N(1)	93.2(3)	88.71(10)
O(6)−Ru(2)−O(7)	88.6(2)	90.49(9)
O(6)−Ru(2)−O(8)	88.7(2)	90.82(9)
O(7)−Ru(2)−O(8)	93.5(3)	92.97(9)
O(6)−Ru(2)−O(10)	91.9(2)	91.20(9)
O(7)−Ru(2)−O(10)	178.2(3)	178.31(9)
O(8)−Ru(2)−O(10)	84.7(3)	86.98(9)
O(6)−Ru(2)−O(9)	174.4(2)	177.24(9)
O(7)−Ru(2)−O(9)	88.9(2)	87.02(9)
O(8)−Ru(2)−O(9)	86.5(3)	88.13(9)
O(9)−Ru(2)−O(10)	90.5(2)	91.29(9)
O(6)−Ru(2)−N(4)	87.1(3)	87.27(10)
O(7)−Ru(2)−N(4)	90.7(3)	85.71(10)
O(8)−Ru(2)−N(4)	173.9(3)	177.66(10)
O(9)−Ru(2)−N(4)	97.9(3)	93.73(10)
O(10)−Ru(2)−N(4)	91.0(3)	94.40(10)

The magnetic interaction between two Ru^{III} ($S = {}^1/_2$) centers is given by the exchange spin Hamiltonian $H = -2JS_1S_2$, which leads to the analytical expression of eq 1 for the magnetic susceptibility.[14]

$$\chi = \frac{Ng^2\beta^2}{kT}\frac{2\exp(2J/kT)}{1+3\exp(2J/kT)} \quad (1)$$

The presence of a temperature-independent paramagnetism (TIP) and that of a paramagnetic impurity (S = 1) have been considered, as shown in eq 2.

$$\chi' = (1-P)(\chi + \mathrm{TIP}) + P\frac{2Ng^2\beta^2}{3kT} \quad (2)$$

The terms N, g, β, k, J, and T in eqs 1 and 2 have the usual meaning, and P is the mole fraction of the noncoupled paramagnetic impurity. The fit of the experimental data using eq 2 gives good agreement between the experimental and calculated curves (Figure 3a). The parameters obtained in the

(10) Sarkar, B.; Patra, S.; Fiedler, J.; Sunoj, R. B.; Janardanan, D.; Mobin, S. M.; Niemeyer, M.; Lahiri, G. K.; Kaim, W. *Angew. Chem., Int. Ed.* **2005**, *44*, 5655.
(11) (a) Patra, S.; Miller, T. A.; Sarkar, B.; Niemeyer, M.; Ward, M. D.; Lahiri, G. K. *Inorg. Chem.* **2003**, *42*, 4707. (b) Koiwa, T.; Masuda, Y.; Shono, J.; Kawamoto, Y.; Hoshino, Y.; Hashimoto, T.; Natarajan, K.; Shimizu, K. *Inorg. Chem.* **2004**, *43*, 6215. (c) Eaton, D. R. *J. Am. Chem. Soc.* **1965**, *87*, 3097. (d) Palmer, R. A.; Fay, R. C.; Piper, T. S. *Inorg. Chem.* **1964**, *3*, 875. (e) Holm, R. H.; Cotton, F. A. *J. Am. Chem. Soc.* **1958**, *80*, 5658. (f) Fay, R. C.; Piper, T. S. *J. Am. Chem. Soc.* **1963**, *85*, 500. (g) Chen, J.-L.; Zhang, X.-U.; Zhang, L.-Y.; Shi, L.X.; Chen, Z.-N. *Inorg. Chem.* **2005**, *44*, 1037.
(12) (a) Kar, S.; Chanda, N.; Mobin, S. M.; Datta, A.; Urbanos, F. A.; Puranik, V. G.; Jimenez-Aparicio, R.; Lahiri, G. K. *Inorg. Chem.* **2004**, *43*, 4911. (b) Kar, S.; Chanda, N.; Mobin, S. M.; Urbanos, F. A.; Niemeyer, M.; Puranik, V. G.; Jimenez-Aparicio, R.; Lahiri, G. K. *Inorg. Chem.* **2005**, *44*, 1571. (c) Chao, G. K. J.; Sime, R. L.; Sime, R. J. *Acta Crystallogr.* **1973**, *B29*, 2845. (d) Sarkar, B.; Laye, R. H.; Mondal, B.; Chakraborty, S.; Paul, R. L.; Jeffery, J. C.; Puranik, V. G.; Ward, M. D.; Lahiri, G. K. *J. Chem. Soc., Dalton Trans.* **2002**, 2097.
(13) Kahn, O. *Molecular Magnetism*; VCH: Weinheim, 1993; p 107.
(14) Carlin, R. L. *Magnetochemistry*, Springer-Verlag: Berlin, 1986; p 14.

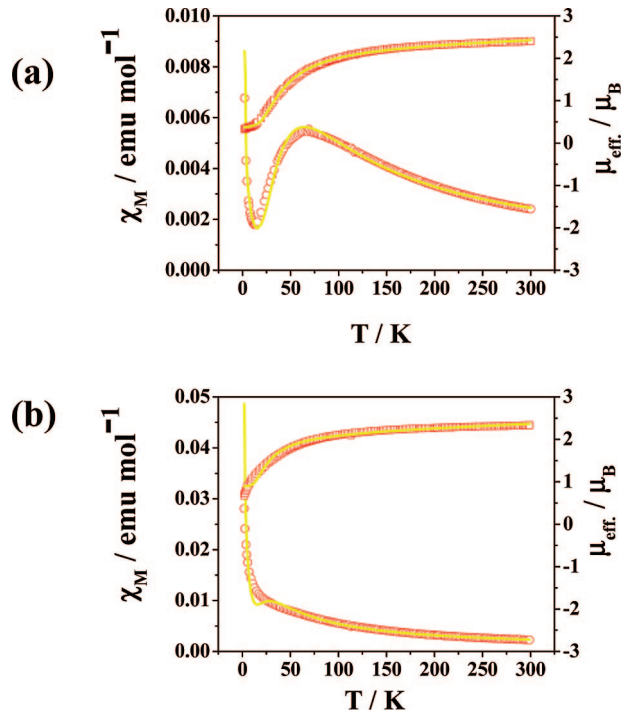

Figure 3. Temperature dependence of the molar susceptibility χ_M (circles) and μ_{eff} (squares) for (a) **1** and (b) **2**. Solid lines are the products of a least-squares fit to the model mentioned in the text.

best fits are $g = 1.89$, $J = -37.14$ cm^{-1}, TIP $= 4.21 \times 10^{-4}$ emu mol^{-1}, $P = 1.64\%$, and $\sigma^2 = 1.23 \times 10^{-4}$ [$\sigma^2 = \sum(\mu_{\text{eff calcd}} - \mu_{\text{eff exptl}})^2/\sum\mu_{\text{eff exptl}}^2$]. The J value of -37.14 cm^{-1} indicates a strong antiferromagnetic interaction between the two diruthenium(III) centers in **1**.

The magnetic moment of complex **2** (*rac* isomer) is 2.33 μ_B at room temperature, which is lower than that expected for two Ru^{III} centers, and it decreases until 0.68 μ_B at 2 K (Figure 3b). This steep decrease indicates a significant antiferromagnetic interaction. Unlike for **1**, the magnetic susceptibility curve for the *rac* isomer **2** does not show any maximum; the susceptibility value increases smoothly with decreasing temperature. The calculated parameters for **2** using eq 2 are $g = 1.68$, $J = -21.07$ cm^{-1}, TIP $= 5.45 \times 10^{-4}$ emu mol^{-1}, $P = 9.86\%$, and $\sigma^2 = 4.41 \times 10^{-4}$. The substantially lower J value of -21.07 cm^{-1} for **2** in contrast to -37.14 cm^{-1} for **1** is in accordance with the maximum observed at 69 K for **1**; the paramagnetic impurity ($S = 1$) in **2** probably obscures the maximum in the experimental susceptibility curve for **2**.

The J and TIP values calculated for **1** and **2** lie in a range similar to that reported for related diruthenium complexes.[15] However, the calculated g values are lower than $g = 2.0$, as observed also in certain other Ru^{III} complexes.[12a,16] The use of $g = 2$ in eq 1 led to poor quality of the fits. The more pronounced spin−spin coupling in **1** occurs in agreement with a slightly shorter Ru−Ru distance and more twisting of the pyrazolyl rings. It is accompanied by broader EPR and ^{1}H NMR signals (Figure S1).

Redox Properties, EPR, and Spectroelectrochemistry. Each of the complexes **1** and **2** shows two successive one-electron oxidation and reduction processes (Table 3 and Figure 4), with a noticeable difference in potentials between the diastereomers.[17] The oxidations and reductions of the *meso* isomer (**1**) take place at relatively more positive and negative potentials, respectively. The potential differences between the successive two-step

Table 3. Redox Potentials[a] and Comproportionation Constants for **1** and **2**

	E°_{298} [V] (ΔE_p [mV])			E°_{298} [V] (ΔE_p [mV])		
compd	couple I	couple II	K_{c1}[b]	couple III	couple IV	K_{c2}[b]
1	0.97 (90)	0.34 (85)	$10^{10.6}$	−1.11 (123)	−1.33 (166)	$10^{3.7}$
2	0.92 (145)	0.25 (98)	$10^{11.3}$	−1.03 (105)	−1.28 (111)	$10^{4.3}$

[a] Potentials E°_{298} [V] (ΔE [mV]) versus SCE; in CH_3CN/0.1 M Et_4NClO_4; scan rate, 100 mV s^{-1}. [b] $RT \ln K_c = nF(\Delta E)$.

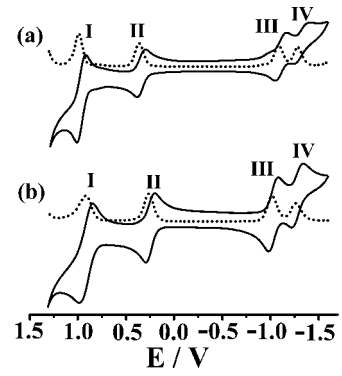

Figure 4. Cyclic voltammograms and differential pulse voltammograms of (a) **1** and (b) **2** in CH_3CN/0.1 M [Et_4N][ClO_4]. Scan rate, 100 mV s^{-1}.

oxidation and reduction processes result in comproportionation constants of $K_{c1} \approx 10^{11}$ and $K_{c2} \approx 10^4$, respectively ($RT \ln K_c = nF\Delta E$).[18] The Ru^{III} centers in **1** and **2** can undergo two successive one-electron oxidations to $Ru^{IV}Ru^{IV}$ and two one-electron reductions to the $Ru^{II}Ru^{II}$ state (eqs 3 and 4), each time via the intermediacy of mixed-valent states, $Ru^{III}Ru^{IV}$ and $Ru^{III}Ru^{II}$.

$$Ru^{III}(\mu\text{-}L^{2-})Ru^{III} \underset{+e^-}{\overset{-e^-}{\rightleftharpoons}} \begin{matrix} Ru^{III}(\mu\text{-}L^{\bullet-})Ru^{III} \\ \text{or} \\ Ru^{III}(\mu\text{-}L^{2-})Ru^{IV} \end{matrix} \underset{+e^-}{\overset{-e^-}{\rightleftharpoons}} \begin{matrix} Ru^{III}(\mu\text{-}L^{0})Ru^{III} \\ \text{or} \\ Ru^{IV}(\mu\text{-}L^{2-})Ru^{IV} \end{matrix} \quad (3)$$

$$Ru^{III}(\mu\text{-}L^{2-})Ru^{III} \underset{-e^-}{\overset{+e^-}{\rightleftharpoons}} Ru^{III}(\mu\text{-}L^{2-})Ru^{II} \underset{-e^-}{\overset{+e^-}{\rightleftharpoons}} Ru^{II}(\mu\text{-}L^{2-})Ru^{II} \quad (4)$$

However, the remarkable mixing of dπ(Ru) and pπ(quinone) orbitals[5,7,19] may also imply the alternative oxidation of L^{2-} to the quinone form via the semiquinone radical intermediate (Scheme 2). Therefore, the challenges were to establish the preferential participation of metal or ligand or mixed metal−ligand orbitals in the spectroscopically accessible oxidation/reduction processes and to characterize possible mixed-valent intermediate configurations with reference to electronic localization (valence trapping) or delocalization (valence averaging).

Oxidation. The EPR signals of the first oxidized species, $\mathbf{1}^+$ or $\mathbf{2}^+$, at about $g = 2.005$ (Figure 5) confirm the preferential

(15) Patra, S.; Sarkar, B.; Maji, S.; Fiedler, J.; Urbanos, F. A.; Jimenez-Aparicio, R.; Kaim, W.; Lahiri, G. K. *Chem. Eur. J.* **2006**, *12*, 489.
(16) Schneider, R.; Weyhermueller, T.; Wieghardt, K.; Nuber, B. *Inorg. Chem.* **1993**, *32*, 4925.
(17) (a) Sarkar, B.; Patra, S.; Fiedler, J.; Sunoj, R. B.; Janardhan, D.; Lahiri, G. K.; Kaim, W. *J. Am. Chem. Soc.* **2008**, *130*, 3532. (b) Maji, S.; Sarkar, B.; Patra, S.; Fiedler, J.; Mobin, S. M.; Puranik, V. G.; Kaim, W.; Lahiri, G. K. *Inorg. Chem.* **2006**, *45*, 1316.
(18) Creutz, C. *Prog. Inorg. Chem.* **1983**, *30*, 1.
(19) Ghumaan, S.; Sarkar, B.; Patra, S.; Parimal, K.; Slageren, J. V.; Fiedler, J.; Kaim, W.; Lahiri, G. K. *Dalton Trans.* **2005**, 706.

Scheme 2

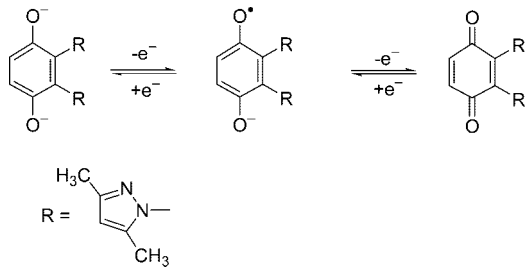

oxidation of L^{2-} to $L^{\bullet-}$ (Scheme 2) over the alternative metal-based redox process, $Ru^{III} \rightarrow Ru^{IV}$, leading to a three-spin situation in $\{Ru^{III}(\mu\text{-}L^{\bullet-})Ru^{III}\}$. Remarkably, strong antiferromagnetic coupling between the terminal, metal-based spins leaves the residual unpaired spin on the central semiquinone, $L^{\bullet-}$ [up−up−down situation ($\uparrow\uparrow\downarrow$, $S = {}^1/_2$) instead of up−up−up ($\uparrow\uparrow\uparrow$, $S = {}^3/_2$) or up−down−up ($\uparrow\downarrow\uparrow$, $S = {}^1/_2$)]. This situation arises most probably because of comparatively weak metal−radical coupling resulting from the pyrazolyl/*p*-semiquinone twist, while the metal−metal antiferromagnetic exchange interaction between the Ru^{III} centers is sizable, as established similarly for the nonoxidized precursors (see above). Otherwise, remaining Ru^{III}-based spin would contribute to yield an EPR spectrum with sizable *g* anisotropy due to the large spin−orbit coupling constant of Ru^{3+}.[7a] Conformation dependence of antiferromagnetic coupling between adjacent spins in a three-spin situation with competing contributions of metal and ligand spins to the total exchange was observed earlier for the "reverse" arrangement $L_{Sq}-Cu^{II}-L_{Sq}$ (L_{Sq} = *o*-semiquinone monoimines).[20,21] Weak coupling in a twisted situation led to ligand-based spin[20] according to ($\uparrow\downarrow\uparrow$), whereas strong antiferromagnetic coupling between the terminal ligand-based spins according to ($\uparrow\uparrow\downarrow$) in a coplanar situation $\{L_{Sq}-Cu^{II}-L_{Sq}\}$ led to metal-based spin, as evident from EPR.[21] In the present case, the free radical EPR signals of the one-electron oxidized species $\mathbf{1}^+$ or $\mathbf{2}^+$ rule out alternative mixed-valent intermediate formulations such as $[(acac)_2Ru^{III}(\mu\text{-}L^{2-})Ru^{IV}(acac)_2]^+$ or the redox redistributed form

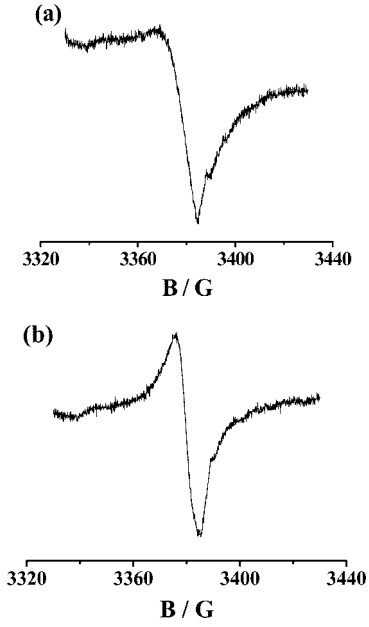

Figure 5. EPR spectra of one-electron-oxidized (a) $\mathbf{1}^+$ and (b) $\mathbf{2}^+$ in CH_3CN/Bu_4NPF_6 at 110 K.

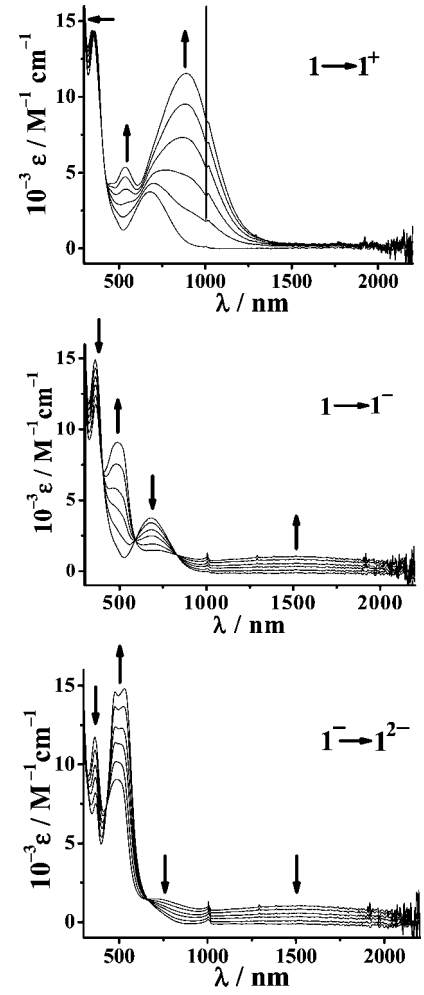

Figure 6. OTTLE spectroelectrochemistry for $\mathbf{1}^n$ in CH_3CN/0.1 M Bu_4NPF_6. Spectra collected during 2 mV/s linear voltammetric scan; curves correspond to potentials: 0.10, 0.30, 0.33, 0.36, 0.40, and 0.55 V (top); −0.85, −1.07, −1.10, −1.13, −1.16, and −1.23 V (middle); −1.23, −1.29, −1.32, −1.34, −1.37, and −1.52 V (bottom).

$[(acac)_2Ru^{III}(\mu\text{-}L^{o})Ru^{II}(acac)_2]^+$, as both such forms should exhibit Ru^{III}-type EPR spectra.

In corroboration of the EPR evidence for the one-electron-oxidized species as semiquinone radical-bridged antiferromagnetically coupled $Ru^{III}Ru^{III}$ states $[(acac)_2\{Ru^{III}(\mu\text{-}L^{\bullet-})Ru^{III}\}(acac)_2]^+$, the cations $\mathbf{1}^+$ and $\mathbf{2}^+$ show relatively broad, low-energy absorptions at 892 and 1027 nm, respectively, typical for semiquinone radical species (Figures 6 and 7, Table 4).[22] The ligand-to-metal charge-transfer (LMCT) transition ($L^{2-} \rightarrow Ru^{III}$) at 706 nm in $\mathbf{2}$ is shifted to 687 nm in $\mathbf{2}^+$ ($L^{\bullet-} \rightarrow Ru^{III}$), while the same transition in moving from $\mathbf{1}$ to $\mathbf{1}^+$ appears to be obscured by the broad envelope of the low-energy absorption centered at 892 nm (Figures 6 and 7, Table 4). Moreover, both $\mathbf{1}^+$ and $\mathbf{2}^+$ exhibit one moderately intense band near 530 nm [$\mathbf{1}^+$, 537 nm ($\varepsilon \approx 5400\ M^{-1}\ cm^{-1}$); $\mathbf{2}^+$, 530 nm ($\varepsilon \approx 5300\ M^{-1}\ cm^{-1}$); Figures 6 and 7, Table 4], which can tentatively be assigned to an intraligand transition, involving

(20) Ye, S.; Sarkar, B.; Lissner, F.; Schleid, Th.; van Slageren, J.; Fiedler, J.; Kaim, W. *Angew. Chem.* **2005**, *117*, 2140; *Angew. Chem., Int. Ed.* **2005**, *44*, 2103.
(21) Chaudhuri, P.; Verani, C. N.; Bill, E.; Bothe, E.; Weyhermueller, T.; Wieghardt, K. *J. Am. Chem. Soc.* **2001**, *123*, 2213.
(22) Ghumaan, S.; Sarkar, B.; Patra, S.; Van Slageren, J.; Fiedler, J.; Kaim, W.; Lahiri, G. K. *Inorg. Chem.* **2005**, *44*, 3210.

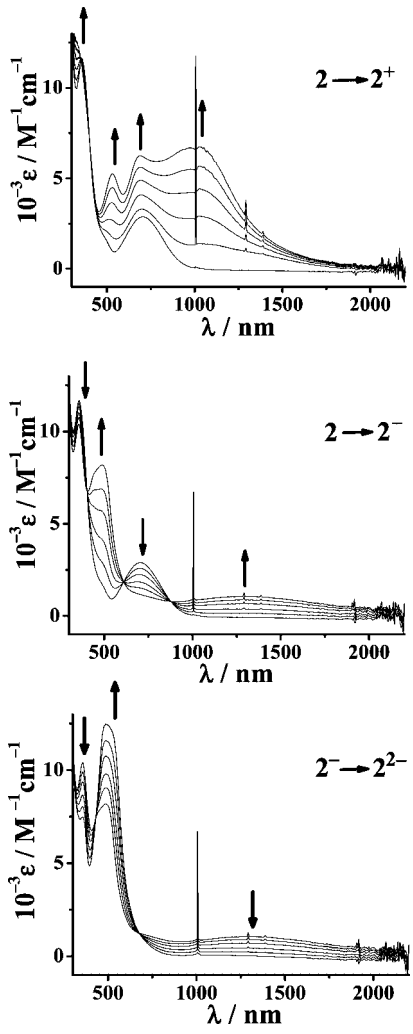

Figure 7. OTTLE spectroelectrochemistry for $\mathbf{2}^n$ in CH_3CN/0.1 M Bu_4NPF_6. Spectra collected during 2 mV/s linear voltammetric scan; curves correspond to potentials: 0.00, 0.20, 0.24, 0.27, 0.30, and 0.45 V (top); −0.80, −0.99, −1.02, −1.05, −1.08, and −1.17 V (middle); −1.17, −1.24, −1.27, −1.30, −1.33, and −1.48 V (bottom).

Table 4. UV−Vis−NIR Data for $\mathbf{1}^n$ and $\mathbf{2}^n$ in Various Oxidation States from OTTLE Spectroelectrochemistry in CH_3CN

compd	λ [nm] (ε [$M^{-1}cm^{-1}$])
$\mathbf{1}^+$	892 (11600), 537 (5400), 346 (14500)
1	681 (3800), 360 (14400)
$\mathbf{1}^-$	1520 (1000, ∼5000[a]), 704 (1470), 510 (8900), 480 (9000), 363 (11800)
$\mathbf{1}^{2-}$	531 (14900), 477 (14600), 369 (7500)
$\mathbf{2}^+$	1027 (6700), 687 (6300), 530 (5300), 335 (12300)
2	706 (2900), 356 (11600)
$\mathbf{2}^-$	1290 (1050, ∼5000[a]), 723 (1100), 492 (8200), 440 (7700), 357 (10400)
$\mathbf{2}^{2-}$	528 (12000), 479 (12400), 359 (7500)

[a] Band width at half-height in cm^{-1}.

the SOMO of the semiquinone bridge. Although the two-electron-oxidized species ($\mathbf{1}^{2+}$ and $\mathbf{2}^{2+}$) appear to be generated reversibly on the cyclic voltammetry time scale (Figure 4), they were not sufficiently stable on the electrolysis time scale. In the case of $[(bpy)_2Ru^{II}(\mu\text{-}L'^{2-})Ru^{II}(bpy)_2]^{2+}$, the first oxidation product was proposed to be $[(bpy)_2Ru^{II}(\mu\text{-}L'^{\bullet-})Ru^{II}(bpy)_2]^{3+}$ via spectroelectrochemistry and resonance Raman studies.[7e] This result is probably favored through the Ru^{II} stabilization by the bpy ancillary ligands. In contrast, the one-electron oxidation of $[(acac)_2Ru^{III}(\mu\text{-}L''^{2-})Ru^{III}(acac)_2]$ (**3**, L''^{2-} = 1,4-dioxido-9,10-anthraquinone) was found to take place at the metal, leading to the formation of mixed-valent $[(acac)_2Ru^{III}(\mu\text{-}L''^{2-})Ru^{IV}(acac)_2]^+$ as suggested by EPR and by a long-wavelength $Ru^{III}\rightarrow Ru^{IV}$ intervalence charge-transfer (IVCT) transition.[7c]

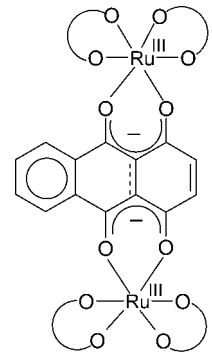

3
rac or meso

Reduction. Since the bridging ligand L^{2-} of **1** or **2** is in the fully reduced form, the observed successive one-electron reductions (Figure 4, Table 3) must be associated with the metals. Consequently, the monoanions $\mathbf{1}^-$ and $\mathbf{2}^-$ exhibit typical Ru^{III}-type rhombic EPR spectra[23] [$\mathbf{1}^-$, $g_1 = 2.40$, $g_2 = 2.19$, $g_3 = 1.79$, $\Delta g = 0.61$, $\langle g\rangle = 2.14$; $\mathbf{2}^-$, $g_1 = 2.41$, $g_2 = 2.19$, $g_3 = 1.77$, $\Delta g = 0.64$, $\langle g\rangle = 2.14$; where $\Delta g = g_1 - g_3$ and $\langle g\rangle = {}^1/_3(g_1^2 + g_2^2 + g_3^2)^{1/2}$;[24] Figure 8), confirming the mixed-valent configuration $[(acac)_2Ru^{III}(\mu\text{-}L^{2-})Ru^{II}(acac)_2]^-$. The EPR profiles of the diastereomers $\mathbf{1}^-$ and $\mathbf{2}^-$ are quite similar. The large Δg value of >0.6 is in agreement with considerable distortion around the metal centers in $\mathbf{1}^-$ and $\mathbf{2}^-$, as suggested also by the structures of **1** and **2** (Figures 1 and 2).

The mixed-valent $\{Ru^{III}(\mu\text{-}L^{2-})Ru^{II}\}$ intermediates $\mathbf{1}^-$ and $\mathbf{2}^-$ exhibit broad $Ru^{II}\rightarrow Ru^{III}$ IVCT transitions with maxima at 1520 and 1290 nm, respectively, which subsequently disappear on further reduction to the isovalent $\{Ru^{II}(\mu\text{-}L^{2-})Ru^{II}\}$ forms of $\mathbf{1}^{2-}$ and $\mathbf{2}^{2-}$ (Figures 6 and 7, Table 4). Using the Hush formula for Class II mixed-valent systems [$\Delta\nu_{1/2}(\text{calcd}) = (2310\nu_{IVCT})^{1/2}$],[25] the calculated band widths at half-height ($\Delta\nu_{1/2}$) for the IVCT bands are 3898 cm^{-1} at 1520 nm (6579 cm^{-1}) for **1** and 4232 cm^{-1} at 1290 nm (7752 cm^{-1}) for **2**, which are reasonably close to the experimental value of about 5000 cm^{-1} for both $\mathbf{1}^-$ and $\mathbf{2}^-$ (Table 4). The Class II behavior of $\mathbf{1}^-$ and $\mathbf{2}^-$ is also suggested by the electrochemical parameters $K_c = 10^{3.7}$ and $10^{4.3}$ (Table 3), respectively.[26] The broad intervalence transitions (Figures 6 and 7) suggest large structural changes associated with IVCT in $\mathbf{1}^-$ or $\mathbf{2}^-$ as expected from a valence-localized situation.

On reduction to $\mathbf{1}^-$ or $\mathbf{2}^-$, the $L^{2-}\rightarrow Ru^{III}$ LMCT transition of **1** or **2** near 700 nm is slightly red-shifted, with a substantial reduction in intensity (Figures 6 and 7, Table 4). This change

(23) Patra, S.; Sarkar, B.; Ghumaan, S.; Fiedler, J.; Kaim, W.; Lahiri, G. K. *Dalton Trans.* **2004**, 754.
(24) Ghumaan, S.; Kar, S.; Mobin, S. M.; Harish, B.; Puranik, V. G.; Lahiri, G. K. *Inorg. Chem.* **2006**, *45*, 2413.
(25) Hush, N. S. *Prog. Inorg. Chem.* **1967**, *8*, 391.
(26) Robin, M. B.; Day, P. *Adv. Inorg. Chem. Radiochem.* **1967**, *10*, 247.

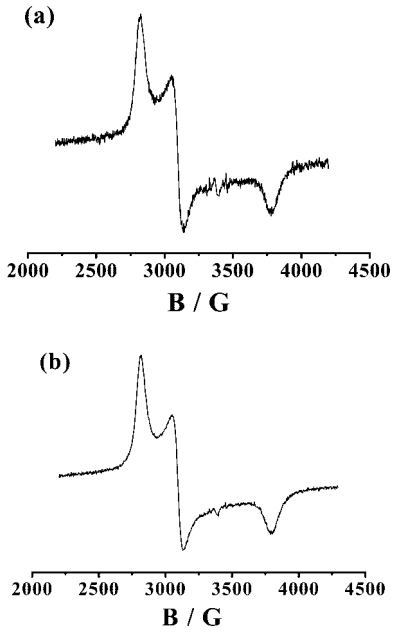

Figure 8. EPR spectra of one-electron-reduced (a) $\mathbf{1}^-$ and (b) $\mathbf{2}^-$ in CH_3CN/Bu_4NPF_6 at 110 K.

is attributed to the presence of only one Ru^{III} center in $\mathbf{1}^-$ or $\mathbf{2}^-$ as opposed to two Ru^{III} ions in **1** or **2**. Consequently, two nearby intense new bands appear in the higher energy region near 500 nm which can be tentatively assigned to MLCT transitions involving filled $(d\pi)Ru^{II}$ and empty π^* orbitals of L^{2-}/$acac^-$. The intensity of the MLCT absorptions increases significantly on further reduction to the isovalent $Ru^{II}Ru^{II}$ state in $\mathbf{1}^{2-}$ or $\mathbf{2}^{2-}$. While we could present here a hydroquinone dianion (L^{2-})-mediated intermetallic electronic coupling in the mixed-valent states $[(acac)_2Ru^{III}(\mu\text{-}L^{2-})Ru^{II}(acac)_2]^-$ ($\mathbf{1}^-$ or $\mathbf{2}^-$), the corresponding 2,5-pyrazolyl-substituted hydroquinone dianion (L'^{2-})- or semiquinone ($L'^{\bullet-}$)-bridged {$Ru(bpy)_2$} termini were reported to exhibit no intermetallic communication.[7e] Nevertheless, we assign a valence-trapped Class II situation to the mixed-valent states in $\mathbf{1}^-$ and $\mathbf{2}^-$, which can be attributed in part to the nonplanarity of the bridging π system of L^{2-}, as evident from the crystal structures of **1** and **2** (Figures 1 and 2).

Differences between Isomers. The identical composition and atom connection of diastereoisomers such as **1** and **2** should allow for detailed insight to be gained into intramolecular electron transfer. While the studies of di- and trinuclear ruthenium complexes with planar redox-active ligands[8a,27] have mostly shown rather small differences between *meso* and *rac* forms, we have reported recently one example where the unusual azo radical-bridged mixed-valent electronic structure led to a significant structural difference.[9,17a,28] The present example involving a *p*-quinonoid ligand makes use of the sterically enforced nonplanarity of the π system of the non-innocent bridge and shows the following differences between diastereoisomers: The *rac* isomer (**2**) exhibits slightly less twisting between the pyrazolyl and hydroquinone dianion planes as well as more regular octahedral configuration at the metals than the *meso* form (**1**). As a consequence of this enhanced intraligand π conjugation in the *rac* alternative, both oxidation and reduction are more facile for **2**, and as a result, the LMCT absorptions of the neutral and oxidized states occur at lower energies for the *rac* isomer. The comproportionation constants of the paramagnetic intermediates are slightly higher for the *rac* forms $\mathbf{2}^+$ and $\mathbf{2}^-$, and the IVCT band appears at higher energy in $\mathbf{2}^-$. The electrochemical and spectroscopic differences thus reflect the less distorted configuration of the *rac* forms with enhanced intraligand π conjugation and more efficient metal−metal electronic interaction. On the other hand, the magnetic (spin−spin) coupling in the neutral forms is weaker for the *rac* isomer **2**, as reflected by NMR, EPR, and susceptibility measurements.

Conclusion

Despite the noted differences between the diastereomeric *meso* and *rac* forms of the structurally identified *p*-quinonoid bridged diruthenium species described here, we could establish a common scheme for their redox behavior, including the determination of the spin and valence situations (Scheme 3). Based in particular on the EPR results, the first oxidation of the neutral forms occurs at the ligand, leading to the formation of mutually antiferromagnetically coupled Ru^{III} ions bridged by a *p*-semiquinone radical. Only the right-hand alternative for the monocations in Scheme 3 is compatible with the experimentally observed ligand-centered spin, supported by the severe structural twist which disfavors alternating metal−ligand−metal antiparallel spin−spin interaction. In other words, the total exchange between the metal spins is antiferromagnetic and of greater magnitude than the total exchange between the organic radical and the Ru^{III}.

There are fewer alternatives available on the reduction side, where successive metal-based one-electron additions result in isovalent diruthenium(II) dianions via the mixed-valent monoanionic intermediates. The moderate intermetallic electronic coupling (Class II) mediated by the nonplanar ligand L^{2-} derived from a substituted *p*-quinone is assumed to occur via a hole-transfer superexchange pathway involving $d\pi(Ru)$ and $p\pi(L^{2-})$ orbitals.[28] Considering these results, it may be expected that suitably modified *p*-quinones can serve increasingly as tunable mediators for valence and spin interaction between metals.

Experimental Section

Materials. The precursor complex $Ru(acac)_2(CH_3CN)_2$ was prepared according to the reported procedure.[29] The ligand precursor 1,4-dihydroxy-2,3-bis(3,5-dimethylpyrazol-1′-yl)benzene (H_2L) was prepared as reported earlier.[30] Other chemicals and solvents were of reagent grade and used as received.

Instrumentation. UV−vis−NIR spectroelectrochemical studies were performed in CH_3CN/0.1 M Bu_4NPF_6 at 298 K using an optically transparent thin-layer electrode (OTTLE) cell[31] mounted in the sample compartment of a J&M TIDAS spectrophotometer. ^1H NMR spectra were obtained with a 400 MHz Varian FT spectrometer. The EPR measurements were made in a two-electrode capillary tube[32] with an X-band (9.5 GHz) Bruker system ESP300 spectrometer. Cyclic voltammetric, differential pulse voltammetric, and coulometric measurements were carried out using a PAR model 273A electrochemistry system. Platinum wire working and auxiliary electrodes and an aqueous saturated calomel reference electrode

(27) (a) Kelso, L. S.; Reitsma, D. A.; Keene, F. R. *Inorg. Chem.* **1996**, *35*, 5144. (b) D'Alessandro, D. M.; Davies, M. S.; Keene, F. R. *Inorg. Chem.* **2006**, *45*, 1656.
(28) Kaim, W.; Lahiri, G. K. *Angew. Chem., Int. Ed.* **2007**, *46*, 1778.
(29) Kobayashi, T.; Nishina, Y.; Shimizu, K. G.; Satô, G. P. *Chem. Lett.* **1988**, 1137.
(30) Catalrin, J.; Fabero, F.; Guijarro, M. S.; Claramunt, R. M.; Santa Maria, M. D.; Foces-Foces, M. C.; Cano, F. H.; Elguero, J.; Sastre, R. *J. Am. Chem. Soc.* **1990**, *112*, 747.
(31) Krejcik, M.; Danek, M.; Hartl, F. *J. Electroanal. Chem.* **1991**, *317*, 179.
(32) Kaim, W.; Ernst, S.; Kasack, V. *J. Am. Chem. Soc.* **1990**, *112*, 173.

Scheme 3

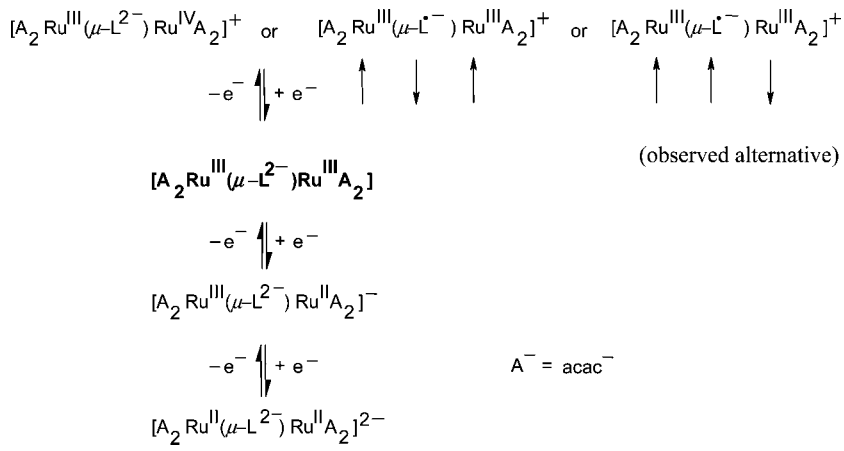

(SCE) were used in a three-electrode configuration. The supporting electrolyte was 0.1 M Et_4NClO_4, and the solute concentration was *ca.* 10^{-3} M. The half-wave potential $E°_{298}$ was set equal to $0.5(E_{pa} + E_{pc})$, where E_{pa} and E_{pc} are anodic and cathodic cyclic voltammetric peak potentials, respectively. Elemental analyses were carried out with a Perkin-Elmer 240C elemental analyzer. Electrospray mass spectra were recorded on a Micromass Q-ToF mass spectrometer.

Crystallography. Single crystals of **1**·$2H_2O$ and **2**·$2CH_2Cl_2$ were grown by slow evaporation of 1:1 dichloromethane−hexane solutions at 298 K. The hydrogen atoms associated with the water molecules in **1**·$2H_2O$ could not be generated. X-ray diffraction data were collected using an Oxford XCALIBUR-S CCD single-crystal X-ray diffractometer. The structures were solved and refined by full-matrix least-squares techniques on F^2 using the SHELX-97 program.[33] The absorption corrections were done by the multiscan technique. All data were corrected for Lorentz and polarization effects, and the non-hydrogen atoms were refined anisotropically. Hydrogen atoms were included in the refinement process as per the riding model.

Magnetic Susceptibility Measurements. The variable-temperature magnetic susceptibilities were measured on polycrystalline samples with a Quantum Design MPMSXL superconducting quantum interference device (SQUID) susceptometer over a temperature range of 2−300 K at a constant field of 10000 G. Each raw data field was corrected for the diamagnetic contribution of both the sample holder and the complex to the susceptibility. The molar diamagnetic corrections were calculated on the basis of Pascal constants. Magnetization measurements were carried out at 5 and 300 K from 0 to 50000 G. The fit of the experimental data was carried out using the MATLAB v.5.1.0.421 program.

Synthesis of [{(acac)$_2$Ru^{III}}$_2$(μ-L^{2-})] (1 and 2). The ligand precursor 1,4-dihydroxy-2,3-bis(3,5-dimethylpyrazol-1′-yl)benzene (H_2L) (40 mg, 0.131 mmol), was added to a 40 mL ethanolic solution of $Ru(acac)_2(CH_3CN)_2$ (100 mg, 0.262 mmol), followed by addition of excess NEt_3 (0.2 mL, 1.31 mmol). The mixture was heated to reflux for 24 h under atmospheric conditions. The initially orange solution gradually changed to deep green. The solvent of the reaction mixture was evaporated under reduced pressure. The residue was purified using a neutral alumina column. Initially, a yellow band of unreacted H_2L followed by a red band of $Ru(acac)_3$ were eluted with CH_2Cl_2. Further elution by CH_2Cl_2−CH_3CN (50:1) gave bright green **1**, and olive green **2** was eluted by CH_2Cl_2−CH_3CN (5:1).

1. Yield, 30 mg (25%). Anal. Calcd (Found): C, 48.25 (48.18); H, 4.99 (5.19); N, 6.25 (6.04). ESI MS (in CH_3CN), *m*/*z* calcd (found) for $[\mathbf{1}]^+$: 896.114 (897.359). ^{1}H NMR in $CDCl_3$ (δ, ppm): −20.00(1H), −19.39(6H), −14.17(6H), −6.96(6H), −5.72(1H), −4.07(6H), −3.67(6H), 1.26 ($CDCl_3$), 3.22(6H), 5.30(2H), 7.29 ($CDCl_3$).

2. Yield, 35 mg (30%). Anal. Calcd (Found): C, 48.25 (48.23); H, 4.99 (5.11); N, 6.25 (6.09). ESI MS (in CH_3CN), *m*/*z* calcd (found) for $[\mathbf{2}]^+$: 896.114 (897.339). ^{1}H NMR in $CDCl_3$ (δ, ppm): −21.22(1H), −19.10(3H), −16.80(3H), −13.57(3H), −10.89(1H), −9.80(1H), −7.36(2H), −7.07(3H), −6.94(3H), −5.05(3H), −4.17(3H), −3.55(3H), −0.85(1H), 1.46 ($CDCl_3$), 5.28(1H), 6.62(3H), 7.25 ($CDCl_3$), 13.11(3H), 22.01(3H), 23.94(3H), 28.23(1H).

Acknowledgment. Financial support received from the Department of Science and Technology and Council of Scientific and Industrial Research (New Delhi, India), the DAAD and the DFG (Germany), and the Spanish MEC (CTQ 2005-00397) and CAM (S-0505-MAT-0303) is gratefully acknowledged.

Supporting Information Available: ^{1}H NMR (EPR inset) spectra of **1** and **2** (Figures S1 and S2), magnetization curve versus magnetic field at 5 and 300 K for **1** and **2** (Figures S3 and S4), and X-ray crystallographic data, in CIF format, for **1** and **2**. This material is available free of charge via the Internet at http://pubs.acs.org.

JA807043S

(33) Sheldrick, G. M. *SHELXS97*, Program for Crystal Structure Solution and Refinement; University of Göttingen: Germany, 1997.